Ashraf, M., Gardner, L. and Nethercot, D. A. (2006). Finite element modelling of structural stainless steel cross-sections. Thin-Walled Structures. **44(10)**, 1048-1062.

Finite element modelling of structural stainless steel cross-sections

Mahmud Ashraf, Leroy Gardner and David A. Nethercot

Department of Civil and Environmental Engineering

Imperial College London, London SW7 2AZ, UK.

Abstract

Stainless steel's characteristic nonlinear, rounded stress-strain behaviour requires accurate recognition in numerical modelling. Its response to cold-working is far more pronounced than that of ordinary carbon steel and hence appropriate modelling of the cold-worked corner regions is very important. Despite the importance of geometrical imperfections, their measurement is not a very common practice and assumed models are generally adopted in numerical investigations – often without proper verification. This paper investigates all important aspects for modelling stainless steel cross-sections through carefully designed parametric studies. Different cross-section types have been considered and the numerically obtained load-deformation responses have been compared with selected experimental results; the findings form the basis for specific guidelines. These proposals have been verified by application to all available stainless steel stub column tests obtained from different sources. The predicted numerical results have shown excellent agreements with those obtained experimentally.

Keywords: Cross-section, Finite element, Geometric imperfection, Numerical modelling, Residual stress, Stainless steel, Structures, Stub column.

1. Introduction

Numerical techniques have now become an invaluable part of most structural research, since they can be employed as an efficient tool for analysing the behaviour of structures provided that suitable care is taken to ensure that the model is appropriate and the input parameters are accurately specified. The sensitivity to changes in these parameters also needs to be properly understood. Since it is not practical to verify all structural design guidance by testing, a better approach is to first conduct some tests, then to replicate the testing procedures using numerical techniques, and, once the numerical models have been verified, to generate further results through variation of appropriate parameters in the numerical model.

A large number of test results have been used in the present study to develop a consistent finite element (FE) modelling technique using the general purpose FE software package ABAQUS [1]. This paper describes the development of the FE models, giving special emphasis to the appropriate guidelines for input parameters such as enhanced strength in the corner regions and the extent of this strength enhancement, initial geometric imperfections and the significance of residual stresses. Extensive parametric studies have been carried out to establish the proposed guidelines, which should assist with modelling of stainless steel structural elements and thus ensure dependable results.

A total of 136 stub columns obtained from 8 different testing programmes involving 4 different grades as well as 6 different cross-section types have been considered in the present study. However, complete load-deformation behaviour was available only for 28 stub columns with 4 different cross-section types and hence these results have been used in performing the parametric studies. The proposed guidelines were, later, used to model the complete set of stub columns to validate the accuracy of the proposed FE modelling technique.

2. Material modelling

The development of an appropriate FE model requires the correct representation of the corresponding material characteristics. Inaccurate or inappropriate modelling of the basic material behaviour will overshadow the performance of even the most refined FE models. Stainless steel exhibits a rounded stress-strain curve and strain hardens to a considerably greater extent than carbon steel, resulting in significant changes in material behaviour during cold-forming processes. This phenomenon leads to enhanced strength properties at the corner regions of stainless steel sections. Special care is required to accurately model the response of stainless steel cross-sections with cold-worked corners.

2.1 Modelling of flat material

The degree of roundness of the stress-strain curve of stainless steel varies from grade to grade, with the austenitic grades demonstrating the greatest nonlinearity and strain

hardening. Most of the commonly adopted models for stainless steel are discussed herein.

2.1.1 Ramberg-Osgood model

Ramberg and Osgood [2] proposed the expression given in Equation 1 for the description of material stress-strain behaviour, where E_0 is Young's modulus and K and n are constants.

$$\varepsilon = \frac{\sigma}{E_0} + K\left(\frac{\sigma}{E_0}\right)^n \tag{1}$$

This basic expression was later modified by Hill [3] to give Equation 2 where R_p is a proof stress and c is the corresponding offset (plastic) strain.

$$\varepsilon = \frac{\sigma}{E_0} + c\left(\frac{\sigma}{R_p}\right)^n \tag{2}$$

In both expressions the total strain is expressed as the summation of elastic and plastic strains which are treated separately. The power function is applied only to the plastic strain. The Ramberg-Osgood expression is a popular material model for nonlinear materials since its constants have physical significance and it also provides a smooth curve for all values of strain with no discontinuities. This expression has been used in an informative Annex of ENV 1999-1-1 [4] for describing the stress-strain behaviour of aluminium. The proof stress was taken as the value corresponding to the 0.2%

plastic strain giving the most familiar form of the Ramberg-Osgood expression as given by Equation 3.

$$\varepsilon = \frac{\sigma}{E_0} + 0.002\left(\frac{\sigma}{\sigma_{0.2}}\right)^n \quad (3)$$

This equation has been found to give excellent predictions of stainless steel material stress-strain behaviour up to the 0.2% proof stress $\sigma_{0.2}$ but greatly over-predicts the stresses beyond that level. Figure 1 shows a typical comparison between a measured stainless steel stress-strain curve and the Ramberg-Osgood equation (Equation 3).

2.1.2 Modified Ramberg-Osgood model proposed by Mirambell and Real

Mirambell and Real [5], as a part of their investigation of the flexural behaviour of stainless steel beams, devised a suitable analytical model for stainless steel stress-strain behaviour. The basic Ramberg-Osgood expression was adopted for stresses up to $\sigma_{0.2}$ where the strain hardening exponent n was determined using the 0.05% proof stress $\sigma_{0.05}$ and $\sigma_{0.2}$. For stresses beyond $\sigma_{0.2}$ a modified Ramberg-Osgood formula was adopted by moving the origin of the basic Ramberg-Osgood expression of Equation 3 from (0, 0) to ($\varepsilon_{t0.2}$, $\sigma_{0.2}$), where $\varepsilon_{t0.2}$ is the total strain at $\sigma_{0.2}$. This is explained in Figure 2 and the proposed relationship is given in Equation 4.

$$\varepsilon = \frac{\sigma - \sigma_{0.2}}{E_{0.2}} + \varepsilon_u\left(\frac{\sigma - \sigma_{0.2}}{\sigma_u - \sigma_{0.2}}\right)^m + \varepsilon_{t0.2} \quad (4)$$

where ε_u is the plastic strain at ultimate strength, and m is an additional strain hardening exponent. $E_{0.2}$ is the tangent stiffness at $\sigma_{0.2}$ which may be obtained using Equation 5.

$$E_{0.2} = \frac{\sigma_{0.2} E_0}{\sigma_{0.2} + 0.002nE_0} \quad (5)$$

The proposed relationship was found to be in good agreement with test results. Use of ultimate stress σ_u and the corresponding strain ε_u in Equation 4, however, makes its application limited to model tension behaviour only.

2.1.3 Extension of modified Ramberg-Osgood model proposed by Rasmussen

Rasmussen [6] adopted Mirambell and Real's proposed [5] model, whereby the basic Ramberg-Osgood equation (Equation 3) is used up to $\sigma_{0.2}$, beyond which Equation 4 applies. Rasmussen [6] proposed that the strain hardening exponent n be determined on the basis of the 0.01% proof stress and $\sigma_{0.2}$. Based on tensile coupon data obtained from [7-13] Rasmussen [6] proposed Equation 6 for the determination of the additional strain hardening exponent m.

$$m = 1 + 3.5\frac{\sigma_{0.2}}{\sigma_u} \quad (6)$$

Further expressions were also provided to determine σ_u (Equation 7) and ε_u (Equation 8) in terms of $\sigma_{0.2}$, E_0 and n.

$$\frac{\sigma_{0.2}}{\sigma_u} = \frac{0.2 + 185(\sigma_{0.2} / E_0)}{1 - 0.0375(n - 5)} \quad (7)$$

$$\varepsilon_u = 1 - \frac{\sigma_{0.2}}{\sigma_u} \quad (8)$$

The resulting model is able to describe the full stress-strain curve for stainless steel alloys by using the three basic parameters $\sigma_{0.2}$, E_0 and n, and has been included in Annex C of prEN 1993-1-4 [14] to provide guidance for the modelling of the material behaviour of stainless steel.

2.1.4 Material model adopted in the present study

Gardner and Nethercot [15] recognised the value of Mirambell and Real's [5] two-stage model but noted that its application was limited to the description of tensile stress-strain behaviour because of its dependency on the ultimate stress σ_u and the corresponding strain ε_u. In compression, such parameters do not exist due to the absence of the necking phenomenon. It was therefore proposed by Gardner [16] that the 1% proof stress $\sigma_{0.1}$ and the corresponding strain $\varepsilon_{t1.0}$ be used in place of the ultimate stress. The resulting model as recently proposed by Gardner and Ashraf [17] is given by Equation 9, which applies for stresses greater than $\sigma_{0.2}$.

$$\varepsilon = \frac{(\sigma - \sigma_{0.2})}{E_{0.2}} + \left(\varepsilon_{t1.0} - \varepsilon_{t0.2} - \frac{\sigma_{1.0} - \sigma_{0.2}}{E_{0.2}} \right) \left(\frac{\sigma - \sigma_{0.2}}{\sigma_{1.0} - \sigma_{0.2}} \right)^{n'_{0.2,1.0}} + \varepsilon_{t0.2} \quad (9)$$

where $\varepsilon_{t0.2}$ and $\varepsilon_{t1.0}$ are the total strains at $\sigma_{0.2}$ and $\sigma_{1.0}$ respectively and $n'_{0.2,1.0}$ is a strain hardening exponent. Equation 9 has been found to give excellent agreement

with measured stress-strain curves in both tension and compression and is adopted in the present study.

Ashraf [18] analysed all available coupon tests performed on stainless steel and proposed specific values for n, $n'_{0.2,1.0}$ and $\sigma_{1.0}/\sigma_{0.2}$ for commonly used stainless steel grades so that Equation 9 can be used with the knowledge of only 2 common parameters – $\sigma_{0.2}$ and E_0. Table 1 lists the values proposed for the coefficients involved.

2.2 Modelling of corner material

The effect of cold-work on the corner material of stainless steel cross-sections has been investigated by Ashraf et al [19] and hence models have been proposed to predict the enhanced corner material strength from a knowledge of the flat material properties and the corner geometry. In most of the cases, Equation 10 has been used to predict the corner material strength. However Equation 11 has also been used in the case of roll-formed sections produced from austenitic Grade 1.4301, where virgin material properties were not available.

$$\sigma_{0.2,c} = \frac{1.881\sigma_{0.2,v}}{\left(\frac{r_i}{t}\right)^{0.194}} \tag{10}$$

$$\sigma_{0.2,c} = 0.82\sigma_{u,f} \tag{11}$$

where $\sigma_{0.2,c}$ is the 0.2% proof stress of the corner material

$\sigma_{0.2,v}$ is the 0.2% proof stress of the virgin material

$\sigma_{u,f}$ is the ultimate stress of the flat material

r_i is the internal corner radius

t is the thickness of the cross-section

In the absence of all sufficient test details to allow the determination of n, $n'_{0.2,1.0}$ and $\sigma_{1.0}/\sigma_{0.2}$ values for corner materials, the values for these parameters were taken to be the same as those for the corresponding flat material.

3. Basic aspects of FE modelling – Boundary conditions and analysis technique

The ends of the stub columns were fixed against all degrees of freedom except for the vertical displacement at the loaded edges. Typical boundary conditions for different cross-section types are shown in Figure 3. Constraint equations were used to ensure that all nodes at the loaded end act as a group to move vertically when a concentrated load was applied to one of the nodes at the top end.

In the present research, elastic linear analysis technique using the *BUCKLING command was employed to obtain the Eigenmodes, which were subsequently used to represent initial geometric imperfections. A 'static stress analysis' method was used to simulate the actual load-deformation response of the stub columns. The nonlinear effects arising from geometric and material nonlinearity were included using the 'NLGEOM' option and *PLASTIC command respectively as stated in ABAQUS [1]. All the stub columns were treated as geometrically nonlinear static problems involving buckling, where the load-displacement response shows a negative stiffness making the structure 'unstable' after reaching the peak load. ABAQUS [1] offers

several techniques to analyse this type of problem and among the available options the ‘modified Riks method’ was chosen because of its simplicity and widespread use in similar applications.

4. Selection of an appropriate element type

Shell elements are generally used to model thin-walled structures. ABAQUS [1] includes general-purpose shell elements as well as elements that are specifically formulated to analyse ‘thick’ and ‘thin’ shell problems. The general-purpose shell elements provide robust and accurate solutions to most applications although, in certain cases, enhanced performance may be obtained using the thin or thick shell elements; for example, if only small strains occur and five degrees of freedom per node are desired. General-purpose shell elements include transverse shear deformation, whilst thin shell elements may be used in cases where transverse shear flexibility is negligible. For homogeneous shells this occurs when the thickness is less than about 1/15 of a characteristic length on the surface of the shell, such as the distance between supports.

Stainless steel structural members are generally modelled using either of the following two shell elements available in ABAQUS: general-purpose S4R [20, 21] or thin-shell S9R5 [5, 22]. Both of these elements were considered in the present research, initially, to find the more suitable one to be used for the parametric studies. Keeping all other parameters the same, only the element type was changed and the resulting load-deformation results have been compared with the tests results. It is worth mentioning that the number of nodes was constant for both the cases, whilst the

number of elements was 4 times higher for models using S4R than the corresponding models using S9R5. The obtained numerical results for the peak load F_u and the corresponding deformation δ_u are compared to the test results in Table 2.

The comparisons show that there is no significant difference between the results obtained using two commonly employed shell elements, except for a few stocky sections for which the load-deformation curves are observed to become very flat near the peak load F_u, making the prediction of δ_u very difficult. However, overall the 9-noded thin shell element S9R5 gives better predictions both in terms of average ultimate load and the corresponding deformation for the considered cases. Moreover this element requires less time to converge to a solution, and hence the thin shell S9R5 element has been used for modelling stainless cross-sections in the present study.

5. Convergence study – selecting a suitable mesh

One of the most important aspects of FE modelling is to identify a suitable mesh size for the accurate modelling of the structural response. Finer meshes are generally preferred to obtain better predictions although there is no general guideline for such fineness, which largely depends on the type of structure and analysis involved. Thus performing a convergence study is a pre-requisite for finding a suitable mesh for any FE investigation. Although finer meshes generally provide better predictions, they make the whole process more expensive in terms of the computational time. A compromise is therefore needed between the required level of accuracy and the cost of a solution.

Two different mesh sizes were used to simulate the load-deformation response of stub columns considered in the present research. For all cross-section types, the number of elements in the finer mesh was 4 times higher than the corresponding coarse mesh. Each of the stub columns was analysed using both of these meshes and the results are given in Table 3. The results show that there is a small improvement in predictions for both peak load F_u and the corresponding deformation δ_u with the finer mesh. No further refinement was attempted since the predictions were found to be in good agreement with the test results and this finer mesh has been adopted in the subsequent FE models.

6. Extent of corner enhancement

Previous research showed that enhanced strength should be included beyond the curved corner of the numerical models to achieve the exact replication of the test results [22]. Karren [23] found that for carbon steel sections the effect of cold-forming extends beyond the corner to a distance approximately equal to the thickness t, whilst Abdel-Rahman and Sivakumaran [24] observed increased yield strengths up to a distance of $0.5\pi r_i$ beyond the corner. Stainless steel exhibits far more pronounced strain hardening than carbon steel and hence it is rather more important to investigate the extent of corner enhancement. Based on the results of a numerical investigation performed on stainless steel roll-formed hollow sections, Gardner [16] observed that if the corner properties are extended up to 2t beyond the curved portion good agreement with test results is obtained.

Most of the open cross-sections considered in the present research were formed by the press-braking process. The manufacturing process has been observed to affect the corner material properties [19] and hence a similar parametric study was carried out to investigate the extent to which corner enhancement continues beyond the curved region in the case of press-braked sections. Keeping all other parameters the same, three different cases were studied – enhanced strength only in the curved corner region, enhanced strength region extended to a distance t beyond the corner and enhanced strength region extended to a distance 2t beyond the corner, as shown in Figure 4. Ultimate load carrying capacity F_u and deformation at ultimate load δ_u for each model are compared to the test results in Table 4.

Table 4 clearly shows that for the press-braked stainless steel sections, the enhanced strength needs to be extended up to t beyond the corner to obtain the best predictions using FE models. The importance of inclusion of enhanced strength corner properties varies with the cross-section slenderness β [25] (which, in turn, influences the ratio of corner area to flat area), showing a more significant effect for the relatively stocky sections with low β. As the section becomes more slender, the ratio of corner area to flat area reduces, local buckling becomes more dominant and the effect of enhanced strength corners loses its significance. All considered stub column models were analysed without any enhanced strength (FE $F_{u,c0}$) and the results were compared to those obtained using corner enhancement up to t (FE $F_{u,ct}$). The results are shown in Figure 5. This figure illustrates the importance of using corner properties in the FE models, especially for the relatively stocky cross-sections. The present research uses enhanced properties up to t and 2t beyond the corner for the press-braked and roll-formed sections respectively.

7. Geometric imperfections

Geometric imperfections are an inseparable property of real steel members, with the potential to significantly influence their structural behaviour. When performing an FE analysis to predict the ultimate load, the model should, in general, include both local and global initial imperfections.

Despite the importance of initial geometrical imperfections, there are no general guidelines for their specification. Predictions are normally conducted by either modelling the structure with an assumed initial out-of-plane deflection or by using assumed small transverse forces. Accurate knowledge of distribution, shape and magnitude of imperfections is a prerequisite for numerically simulating the response of a structural member. In the absence of suitable measured data, the magnitude and distribution of imperfections – which is likely to be a complex function of the rolling and fabrication process, material strength and geometrical properties of the cross-section – must be predicted. The present study aims to provide guidelines for predicting the shape and magnitude of initial imperfections for stainless steel stub columns for use in FE modelling.

7.1 Literature review

A detailed review of measured and predicted geometric imperfections in steel cross-sections has been reported in [18]. The most commonly adopted technique to define the distribution of initial imperfections is to perform an elastic buckling analysis prior

to the non-linear analysis and to use one of the Eigenmodes, chosen depending on specific criteria, as the initial shape. The main challenge is to select an appropriate Eigenmode to represent the imperfect geometry of the structural component and to ensure that no buckling modes are inhibited. The maximum amplitude is often taken as a percentage of plate thickness; this type of relationship is, however, always likely to be case sensitive and no specific approach has, so far, been reported that is generally applicable. It should be noted that the initial geometric imperfections in numerical simulations are often employed not just to represent the imperfect geometry of the physical structural element, but also to account for other features such as residual stresses, non-homogeneity of material, eccentricity of loading etc., which may be difficult to model explicitly. Therefore, the choice of maximum amplitude of imperfection, for example, will depend on whether or not these other features have been explicitly incorporated into the model.

Table 5 presents a summary of the previous research performed on geometric imperfections, where t is the plate thickness, ω_0 is the imperfection amplitude, $\sigma_{0.2}$ and σ_{cr} are 0.2% proof stress of material and (elastic) critical plate buckling stress respectively.

7.2 Modelling of distribution and magnitude

The load-deformation responses of stainless steel stub columns with angle, channel, lipped channel and I sections reported by Kuwamura [34] and Stangenberg [35] have been used to investigate the effect of initial imperfections on structural response. No imperfection measurements were available for the stub columns considered and hence

numerically obtained load-deformation curves were compared to those obtained experimentally.

The most commonly used technique, employing Eigenmodes to define the initial geometry of a structure, was adopted in the present work. The Eigenmodes were obtained from elastic buckling analyses of the stub column models. The worst imperfection shape, resulting in the greatest reduction in load-carrying capacity, often relates to the lowest Eigenmode, though it is not always the case. Figure 6 shows some typical Eigenmodes obtained for all the cross-section types considered. In this study, each of the first three Eigenmodes was used individually to investigate the effect of imperfection distribution on load-deformation response. Figure 7 shows the typical load-deformation behaviour for stub columns as a result of changing the shape of the imperfection distribution.

In ABAQUS [1], the nodal displacements of an Eigenmode are normalised using the maximum displacement that occurs within a structure and thus the maximum displacement is set equal to 1. By specifying an appropriate multiplying factor, commonly known as the amplitude, the nodal co-ordinates of the Eigenmode under consideration are scaled accordingly. The present study is also concerned with devising a representative value for the amplitude to be used in the imperfection distribution defined using Eigenmodes. Schafer and Peköz's [28] proposals for this amplitude have been used by various researchers, but were originally devised for carbon steel cross-sections and should be examined before use for stainless steel. Gardner and Nethercot's [22] proposed relationship for imperfection amplitude includes both material and geometrical properties and gave good predictions for roll-

formed stainless steel sections. Initial imperfections for all the stub columns considered in the present study were modelled using these two approaches and were compared with the test results. The obtained FE results are compared and discussed in the following section.

7.3 Results and analysis

Each stub column was analysed six times, including (separately) 3 Eigenmodes (Eigenmodes 1, 2 and 3) and 2 imperfection amplitudes; the load-deformation results are compared in Tables 6 and 7. The mean prediction of test results and coefficient of variation (COV) from the obtained FE results were also calculated and reported. From the scatter (COV) of results it may be observed that the peak load F_u is less sensitive to imperfection shape than is the corresponding deformation δ_u. For the imperfection amplitude, Gardner and Nethercot's [22] proposed technique gives relatively consistent results and predictions closer to the test results than Schafer and Peköz's [28] proposed method. The best prediction is obtained when Eigenmode 1 is used in conjunction with the amplitude taken from Gardner and Nethercot's [22] proposal. Angle sections were observed to be the most sensitive type of cross-section to the chosen imperfection mode.

8. Residual Stresses

Residual stresses are induced into cold-formed stainless steel members as a result of the deformations during the cold-forming process and due to the thermal gradients that occur during welding. Due to the inherent uncertainty associated with the

magnitude and distribution of residual stresses, their effect is often taken into account in numerical models with an appropriate increase in the magnitude of assumed initial geometric imperfections [35].

Both Rasmussen and Hancock [7-8] and Gardner [16] observed that the tension and compression coupons cut from finished sections were curved longitudinally because of the through-thickness bending residual stresses. During testing, however, the coupons are straightened, which effectively re-introduces the bending residual stress into the coupons. Therefore, provided the material properties are established using coupons cut from within the cross-section, the effects of bending residual stresses are inherently present, and do not need to be defined explicitly in the numerical models. It is only the membrane stresses induced through welding that need to be explicitly defined in numerical models.

Lagerqvist and Olsson [36] measured residual stresses in two welded I girders of austenitic and duplex stainless steel. The resulting residual stress patterns resembled established models for carbon steel, but no specific guidelines were proposed. In the case of angles, channels and lipped channels no residual stresses were included in the numerical models. However, in the case of the welded I sections, the thermally induced residual stresses were modelled following the established guidelines for carbon steel [37], as shown in Figure 8, since no specific guidance is available for stainless steel. The 0.2% proof stress $\sigma_{0.2}$ was adopted for stainless steel in place of the yield stress σ_y.

Each of the I section stub columns was modelled twice – with and without residual stresses. The FE results are compared to the test results in Table 8. From the numerically obtained results it may be observed that the effect of residual stresses on the peak load F_u and the corresponding deformation δ_u is not very significant. However, inclusion of residual stress was observed to cause small reductions in the stiffness of the stub columns, which resulted in higher values for δ_u. Overall, it may be observed from the cases considered that the developed numerical models can accurately predict the stub column load-deformation response without explicit recognition of thermal residual stresses. Gardner and Nethercot [22] reached a similar conclusion when modelling stainless steel hollow sections.

9. Proposed technique for numerical modelling and its verification

The following proposals are made for use in the numerical modelling of stainless steel stub columns:

(i) Material behaviour may be accurately modelled using Equations 3 and 9 with the required parameters taken from Table 1.

(ii) Corner material strength $\sigma_{0.2,c}$ should be incorporated for cold-formed sections and may be obtained using either Equation 10 or 11. To obtain the complete stress-strain response, the modified Ramberg-Osgood parameters may be taken from Table 1 if they are not available from corner coupons. The corner enhancement should be extended up to t for the press-braked sections and 2t for

roll-formed sections beyond the curved corner portions, where t is the plate thickness.

(iii) The thin-shell S9R5 element available in ABAQUS [1] has been observed to perform very well for the stub columns considered. The general purpose S4R also provides a similar level of accuracy. A convergence study is a pre-requisite to obtain accurate predictions.

(iv) Initial geometric imperfections in stub columns may be modelled using an appropriate deformed shape obtained from elastic buckling analysis (i.e. Eigenmodes). Eigenmode 1 may be used with an amplitude of $\omega_0 = 0.023(\sigma_{0.2}/\sigma_{cr})t$ to obtain accurate predictions for load-deformation behaviour, where $\sigma_{0.2}$ is the 0.2% proof stress of the material, σ_{cr} is the (elastic) critical plate buckling stress and t is the plate thickness.

(v) Bending residual stresses may be ignored in FE models if the material properties are taken from the coupons cut from the finished cross-section. Thermal residual stresses have been found to have an insignificant effect on the peak load and hence can be omitted if an accurate distribution is unknown.

The aforementioned guidelines have been used to model all 136 stainless steel stub column tests available to date. A summary of the results is given in Table 9, whilst Figure 9 illustrates how the FE versus test prediction varies with cross-section slenderness β. It is worth mentioning that the slenderness parameter β includes both material and cross-sectional properties [25].

Given the variability in cross-section types, manufacturing processes and sources for the considered 136 stub columns, the overall mean prediction of 1.01 with a coefficient of variation (COV) of 0.08 for the peak load F_u may be considered to be acceptable. It should also be noted that the maximum scatter of prediction was observed for the welded cross-sections reported in [34]. In Kuwamura's [34] testing programme, the I sections were welded by laser beam and TIG welding, whilst the SHS sections were formed in a rather unusual fashion – two press-braked channel sections were welded tip-to-tip using laser beam. It is well known that welding can result in high residual stresses, distortion of cross-sections and localised reduction in material strength (when welding cold-worked sections). Coupled with this, only limited material data were available for Kuwamura's [34] tested cross-sections, which, given that significant variability in material properties can exist around structural stainless steel sections [38], creates further uncertainties.

A limited number of failure modes was available for the considered stub columns. However, excellent agreement has been observed between the numerical and experimental deformed shapes. Figure 10 presents some typical failure modes for the different cross-section types.

10. Conclusions

Numerical modelling techniques for stainless steel cross-sections have been explained in detail, giving specific guidelines for the modelling of corner regions, initial imperfections and residual stresses. The numerical models for the press-braked and

the roll-formed stainless steel cross-sections produce the closest predictions to the tests when the enhanced corner properties are used up to a distance equal to or twice the plate thickness respectively, beyond the corner region. The initial imperfection distribution can be modelled using the first Eigenmode with the corresponding amplitude $\omega_0 = 0.023(\sigma_{0.2}/\sigma_{cr})t$. Thermal residual stresses have been observed not to have any significant effect on stub column resistance, and therefore may, in general, be ignored. The performance of all numerical models has been compared to the experimentally obtained load-deformation response and failure modes, where available. The obtained overall mean prediction for the resistance of 136 stub columns considered was 1.01 with a COV of 0.08, which demonstrates the accuracy of the proposed numerical technique.

Acknowledgements

The authors would like to acknowledge the financial support provided by the Commonwealth Scholarship Commission in this research.

References

[1] ABAQUS (2003). ABAQUS/ Standard User's Manual Volumes I-III and ABAQUS Post Manual. Version 6.4. Hibbitt, Karlsson & Sorensen, Inc. Pawtucket, USA.

[2] Ramberg, W. and Osgood, W. R. (1943). Description of stress-strain curves by three parameters. *Technical Note No. 902, National Advisory Committee for Aeronautics.* Washington, D.C.

[3] Hill, H. N. (1944). Determination of stress-strain relations from the offset yield strength values. *Technical Note No. 927, National Advisory Committee for Aeronautics,* Washington, D.C.

[4] ENV 1999-1-1 (1998). Eurocode 9: Design of Aluminium Structures. Part 1.1: General rules – General rules and rules for buildings. CEN.

[5] Mirambell, E. and Real, E. (2000). On the calculation of deflections in structural stainless steel beams: an experimental and numerical investigation. *Journal of Constructional Steel Research*. **54** : 109-133.

[6] Rasmussen, K. J. R. (2003). Full-Range Stress-Strain Curves for Stainless Steel Alloys. *Journal of Constructional Steel Research*. **59**: 47-61.

[7] Rasmussen, K. J. R. and Hancock, G. J. (1993a). Design of cold-formed stainless steel tubular members. I: Columns. *Journal of Structural Engineering.* ASCE ;**119** (8) : 2349-2367.

[8] Rasmussen, K. J. R. and Hancock, G. J. (1993b). Design of cold-formed stainless steel tubular members. II: Beams. *Journal of Structural Engineering.* ASCE ;**119** (8) : 2368-2386.

[9] Talja, A. and Salmi, P. (1995). Design of stainless steel RHS beams, columns and beam-columns. *Research Note 1619*. VTT Building Technology, Finland.

[10] Korvink, S. A., van den Berg, G. J. and van der Merwe, P. (1995). Web crippling of stainless steel cold-formed beams. *Journal of Constructional Steel Research*. **34** : 225-248.

[11] Macdonald, M., Rhodes, J. and Taylor, G. T. (2000). Mechanical properties of stainless steel lipped channels. *Proceedings of the Fifteenth International Specialty Conference on Cold-Formed Steel Structures.* St. Louis, Missouri, U.S.A. 673-681.

[12] Olsson, A. (2001). Stainless steel plasticity – material modelling and structural applications. *Ph.D. Thesis, Department of Civil and Mining Engineering, Luleå University of Technology, Sweden.*

[13] Burns, T. (2001). Buckling of stiffened stainless steel plates. *BE (Honours) Thesis, Department of Civil Engineering, University of Sydney, Australia.*

[14] prEN 1993-1-4 (2004). Eurocode 3: Design of Steel Structures. Part 1.4: General rules - Supplementary rules for stainless steel. CEN.

[15] Gardner, L. and Nethercot, D. A. (2001). Numerical modelling of cold-formed stainless steel sections, *NSCC 2001 proceedings: NSCC 2001 9th Nordic steel construction conference*, Helsinki, Finland, 781 – 790.

[16] Gardner, L (2002). A new approach to structural stainless steel design. *Ph.D. Thesis.* Structures Section, Department of Civil and Environmental Engineering. Imperial College London, UK.

[17] Gardner, L. and Ashraf, M. (2006). Structural design for non-linear metallic materials. *Engineering Structures.* **28**(6): 925-936.

[18] Ashraf, M. (2006). Structural stainless steel design: Resistance based on deformation capacity. *Ph.D. thesis*. Department of Civil and Environmental Engineering, Imperial College London, UK.

[19] Ashraf, M., Gardner, L. and Nethercot, D. A. (2005). Strength enhancement of the corner regions of stainless steel cross-sections. *Journal of Constructional Steel Research.* **61**(1): 37-52.

[20] Lecce, M. and Rasmussen, K. J. R. (2006). Distortional Buckling of Cold-Formed Stainless Steel Sections: Finite-element Modelling and Design. *Journal of Structural Engineering ASCE,* **132**(4): 505-514.

[21] Ellobody, E. and Young B. (2005). Structural performance of cold-formed high strength stainless steel columns. *Journal of Constructional Steel Research*. **61**(12): 1631-1649.

[22] Gardner, L. and Nethercot, D. A. (2004). Numerical modelling of stainless steel structural components - A consistent approach. *Journal of Structural Engineering ASCE*, **130**(10): 1586-1601.

[23] Karren, K. W. (1967). Corner properties of cold-formed steel shapes. *Journal of Structural Engineering, ASCE.* **93**(ST1): 401-432.

[24] Abdel-Rahman, N. and Sivakumaran, K. S. (1997). Material properties models for analysis of cold-formed steel members. *Journal of Structural Engineering* ASCE. **123** (9): 1135-1143.

[25] Ashraf, M., Gardner, L. and Nethercot, D. A. (2006). Compression strength of stainless steel cross-sections. *Journal of Constructional Steel Research*. **62**(1-2) : 105 – 115.

[26] Dawson, R. G. and Walker, A. C. (1972). Post-buckling of geometrically imperfect plates. *Journal of Structural Engineering. ASCE*. **98** (ST1) : 75 – 94.

[27] Hopperstad, O. S., Langseth, M. and Hanssen, L. (1997). Ultimate compressive strength of plate elements in Aluminium: Correlation of Finite Element analyses and tests. *Thin-Walled Structures.* **29**: 31 – 46.

[28] Schafer, B. W. and Peköz, T. (1998). Computational modelling of cold-formed steel: Characterizing geometric imperfections and residual stresses. *Journal of Constructional Steel Research.* **47**: 193 – 210.

[29] Sun, J. and Butterworth, J. W. (1998). Behaviour of steel single angle compression members axially loaded through one leg, *Proceedings of the Australian Structural Engineering Conference.* Auckland, 859 – 866.

[30] Chou, S. M., Chai, G. B. and Ling, L. (2000). Finite element technique for design of stub columns. *Thin-Walled Structures*. **37**: 97 – 112.

[31] Kaitila, O. (2002). Imperfection sensitivity analysis of lipped channel columns at high temperatures. *Journal of Constructional Steel Research.* **58**: 333 – 351.

[32] Dubina, D. and Ungureanu, V. (2002). Effect of imperfections on numerical simulation of instability behaviour of cold-formed steel members. *Thin-Walled Structures.* **40**: 239 – 262

[33] Cruise, R. and Gardner, L. (2006). Measurement and prediction of geometric imperfections in structural stainless steel members. *Structural Engineering and Mechanics*. (In press)

[34] Kuwamura, H. (2003). Local buckling of thin-walled stainless steel members. Steel Structures. **3**: 191-201.

[35] Stangenberg, H. (2000). Development of the use of stainless steel in construction: Work package 2: Cross-sections – Welded I sections and cold formed sheeting. *ECSC Report.*

[36] Lagerqvist, O. and Olsson, A. (2001). Residual stresses in welded I-girders made of stainless steel and structural steel. *Proceedings of the 9th Nordic Steel Construction Conference.* Helsinki, Finland, 737 – 744.

[37] European Convention for Constructional Steelwork ECCS (1984). Ultimate limit state calculation of sway frames with rigid joints. Technical Committee 8 – Structural Stability Technical Working Group 8.2 – System. Publication No. 33.

[38] Young, B. and Lui, W. M. (2005). Behaviour of cold-formed high strength stainless steel sections. *Journal of Structural Engineering. ASCE.* **131**(11) : 1738 – 1745.

Table 1: Compound Ramberg-Osgood parameters obtained from coupon test results.

Type	Grade	Forming process	Tension / Compression	n	$n'_{0.2,1.0}$	$\sigma_{1.0}/\sigma_{0.2}$
Austenitic	1.4301	Press-braked	Tension	5.8	2.7	1.20
			Compression	5.3	2.5	1.20
		Roll-formed	Tension	5.4	3.4	1.14
			Compression	4.3	2.7	1.25
	1.4306, 1.4318	-	-	4.4	3.1	1.17
Ferritic	1.4016	-	-	6.4	3.2	1.16
	1.4003, 1.4512	-	-	7.3	3.3	1.14
Duplex	1.4462	-	-	5.0	3.4	1.15

Table 2: Load-deformation results obtained from FE models of stub columns using general purpose shell element S4R and thin-shell element S9R5.

Section type	Designation	Test Results		General purpose shell element: S4R		Thin-shell element: S9R5	
		F_u (kN)	δ_u (mm)	FE F_u / Test F_u	FE δ_u / Test δ_u	FE F_u / Test F_u	FE δ_u / Test δ_u
Angle	25 × 25 × 3	55.9	1.28	0.94	1.00	0.90	0.98
	30 × 30 × 3	59.4	0.70	0.99	1.27	0.97	1.20
	40 × 40 × 3	66.9	0.50	1.01	1.10	1.00	1.10
	40 × 40 × 3	65.6	0.45	1.04	1.27	1.03	1.31
	50 × 50 × 3	68.7	0.31	1.03	1.29	1.03	1.32
	60 × 60 × 3	69.6	0.25	1.05	1.24	1.06	1.24
Channel	50 × 25 × 3	106.0	2.10	1.04	1.77	0.95	1.29
	80 × 40 × 3	134.2	1.10	1.02	1.17	1.00	1.15
	100 × 50 × 3	146.2	0.90	1.02	0.93	1.01	0.93
	100 × 50 × 3	140.4	0.83	1.07	1.02	1.06	1.04
	150 × 50 × 3	156.0	0.85	0.99	0.87	0.99	0.84
	50 × 50 × 3	125.0	0.72	1.02	1.00	1.02	1.11
Lipped Channel	100 × 50 × 20 × 3	211.4	1.50	1.03	1.24	1.02	1.27
	150 × 50 × 20 × 3	197.0	1.60	1.02	0.96	1.00	0.93
	150 × 65 × 20 × 3	214.8	1.20	1.07	1.42	1.05	1.19
	200 × 75 × 25 × 3	232.8	1.40	1.03	1.21	1.02	1.14
	33 × 17 × 7 × 1	23.7	0.62	0.98	0.84	0.98	0.89
	50 × 17 × 7 × 1	21.7	0.50	1.05	1.04	1.04	0.98
	50 × 22 × 7 × 1	24.3	0.60	1.05	1.02	1.01	0.98
	68 × 25 × 8 × 1	26.1	0.62	1.06	1.29	1.05	1.31
I section	50 × 50 × 3 × 3	151.8	2.40	0.94	1.29	0.89	1.21
	50 × 100 × 3 × 3	190.7	0.73	0.95	1.18	0.94	1.12
	100 × 50 × 3 × 3	170.6	1.34	0.93	1.25	0.91	1.10
	100 × 75 × 3 × 3	199.2	1.07	0.97	1.08	0.96	1.08
	100 × 100 × 3 × 3	201.5	0.49	1.05	1.45	1.04	1.45
	150 × 100 × 3 × 3	200.0	0.61	1.12	1.20	1.12	1.20
	200 × 100 × 3 × 3	206.8	0.80	1.02	1.00	1.02	1.00
	200 × 150 × 3 × 3	230.4	0.89	1.04	1.20	1.03	1.12
All Sections			**Average**	**1.02**	**1.16**	**1.00**	**1.12**
			COV	**0.04**	**0.17**	**0.05**	**0.13**

Table 3: Load-deformation results obtained from FE models of stub columns using different meshes.

Section type	Designation	Test Results		Coarse mesh		Fine mesh	
		F_u (kN)	δ_u (mm)	FE F_u / Test F_u	FE δ_u / Test δ_u	FE F_u / Test F_u	FE δ_u / Test δ_u
Angle	25 × 25 × 3	55.9	1.28	0.90	0.99	0.90	1.00
	30 × 30 × 3	59.4	0.70	0.95	1.19	0.97	1.20
	40 × 40 × 3	66.9	0.50	0.96	1.00	1.00	1.10
	40 × 40 × 3	65.6	0.45	1.01	1.24	1.03	1.29
	50 × 50 × 3	68.7	0.31	1.02	1.35	1.03	1.29
	60 × 60 × 3	69.6	0.25	1.06	1.24	1.06	1.24
Channel	50 × 25 × 3	106.0	2.10	0.96	1.35	0.95	1.29
	80 × 40 × 3	134.2	1.10	1.01	1.12	1.01	1.15
	100 × 50 × 3	146.2	0.90	1.01	0.98	1.01	0.97
	100 × 50 × 3	140.4	0.83	1.06	0.98	1.06	1.00
	150 × 50 × 3	156.0	0.85	0.99	0.86	0.99	0.86
	50 × 50 × 3	125.0	0.72	1.02	1.03	1.02	1.03
Lipped Channel	100 × 50 × 20 × 3	211.4	1.50	1.03	1.31	1.02	1.27
	150 × 50 × 20 × 3	197.0	1.60	1.02	0.93	1.00	0.93
	150 × 65 × 20 × 3	214.8	1.20	1.07	1.55	1.05	1.19
	200 × 75 × 25 × 3	232.8	1.40	1.04	1.28	1.02	1.14
	33 × 17 × 7 × 1	23.7	0.62	0.98	0.90	0.98	0.89
	50 × 17 × 7 × 1	21.7	0.50	1.05	1.08	1.04	1.00
	50 × 22 × 7 × 1	24.3	0.60	1.04	1.05	1.01	1.00
	68 × 25 × 8 × 1	26.1	0.62	1.06	1.29	1.05	1.31
I section	50 × 50 × 3 × 3	151.8	2.40	0.88	1.16	0.89	1.21
	50 × 100 × 3 × 3	190.7	0.73	0.93	1.19	0.94	1.12
	100 × 50 × 3 × 3	170.6	1.34	0.91	1.13	0.91	1.10
	100 × 75 × 3 × 3	199.2	1.07	0.96	1.06	0.96	1.08
	100 × 100 × 3 × 3	201.5	0.49	1.04	1.57	1.04	1.45
	150 × 100 × 3 × 3	200.0	0.61	1.11	1.34	1.12	1.20
	200 × 100 × 3 × 3	206.8	0.80	1.04	1.08	1.02	1.00
	200 × 150 × 3 × 3	230.4	0.89	1.05	1.13	1.03	1.12
All Sections			**Average**	**1.01**	**1.16**	**1.00**	**1.12**
			COV	**0.06**	**0.16**	**0.05**	**0.13**

Table 4: Load-deformation results obtained from FE models of press-braked stub columns using different conditions for corner strength enhancement.

Section type	Designation	Test Results		Extent of enhanced strength used in FE models					
				Corner only		Up to t beyond corner		Up to 2t beyond corner	
		F_u (kN)	δ_u (mm)	FE F_u/ Test F_u	FE δ_u/ Test δ_u	FE F_u/ Test F_u	FE δ_u/ Test δ_u	FE F_u/ Test F_u	FE δ_u/ Test δ_u
Angle	25 × 25 × 3	55.9	1.28	0.81	0.99	0.90	1.00	0.96	0.77
	30 × 30 × 3	59.4	0.70	0.88	1.13	0.97	1.20	1.01	1.14
	40 × 40 × 3	66.9	0.50	0.93	1.02	1.00	1.10	1.01	0.96
	40 × 40 × 3	65.6	0.45	0.96	1.16	1.03	1.29	1.06	1.31
	50 × 50 × 3	68.7	0.31	0.99	1.23	1.03	1.29	1.04	1.35
	60 × 60 × 3	69.6	0.25	1.04	1.20	1.06	1.24	1.07	1.32
Channel	50 × 25 × 3	106.0	2.10	0.88	1.61	0.95	1.29	1.05	1.40
	80 × 40 × 3	134.2	1.10	0.95	1.13	1.01	1.15	1.07	1.27
	100 × 50 × 3	146.2	0.90	0.98	0.89	1.01	0.97	1.07	1.00
	100 × 50 × 3	140.4	0.83	1.02	1.00	1.06	1.00	1.12	1.13
	150 × 50 × 3	156.0	0.85	0.98	0.82	0.99	0.86	0.99	0.86
	50 × 50 × 3	125.0	0.72	0.98	1.00	1.02	1.03	1.09	1.24
Lipped Channel	100 × 50 × 20 × 3	211.4	1.50	0.93	1.19	1.02	1.27	1.11	1.38
	150 × 50 × 20 × 3	197.0	1.60	0.96	0.63	1.00	0.93	1.09	1.04
	150 × 65 × 20 × 3	214.8	1.20	1.00	1.00	1.05	1.19	1.14	1.73
	200 × 75 × 25 × 3	232.8	1.40	0.97	1.02	1.02	1.14	1.10	1.43
	33 × 17 × 7 × 1	23.7	0.62	0.90	0.79	0.98	0.89	1.06	0.90
	50 × 17 × 7 × 1	21.7	0.50	0.97	0.64	1.04	1.00	1.15	1.28
	50 × 22 × 7 × 1	24.3	0.60	0.98	0.55	1.01	1.00	1.12	1.27
	68 × 25 × 8 × 1	26.1	0.62	0.98	1.00	1.02	1.31	1.13	1.42
All Sections			**Average**	**0.95**	**1.00**	**1.01**	**1.11**	**1.07**	**1.21**
			COV	**0.06**	**0.24**	**0.04**	**0.13**	**0.05**	**0.19**

Table 5: Summary of the previous research performed on local geometric imperfections.

Researcher	Structural component/configuration	Experimental/ Numerical	Imperfection model proposed/used		Comment
			shape	magnitude	
Dawson and Walker [26]	Simply supported steel plates under compression and bending.	Experimental	-	$\omega_0/t = \alpha (\sigma_y/\sigma_{cr})^{0.5}$ $\omega_0/t = \gamma (\sigma_y/\sigma_{cr})$	Proposed imperfections can be used in designing cold-formed steel sections.
Hopperstad et al. [27]	Aluminium cruciform sections under compression.	Numerical	$\omega = \omega_0$ (y/b)cos(πx/L)	0.01t to 0.1t	Stocky plates are more sensitive to imperfection amplitude.
Schafer and Peköz [28]	Cold-formed steel lipped channels	Experimental	Eigenmodes	$\omega_0 = 0.006w$ $\omega_0 = 6te^{-2t}$	Periodicity was observed in imperfection distribution.
Sun and Butterworth [29]	Roll-formed steel angles subjected to eccentric compression.	Experimental and numerical	Half sine waves	0.167t, 0.333t, 0.5t and 0.667t	Amplitude of 0.333t observed to give best results.
Chou et al. [30]	Cold-formed steel lipped channels and hat sections under compression.	Numerical	Eigenmodes	0.1t, 0.5t and [26]	Dawson and Walker's [26] proposed method with $\alpha = 0.3$ gave consistent results.
Gardner [16]	Roll-formed stainless steel hollow sections under compression	Experimental and numerical.	1st Eigenmode	$\omega_0/t = 0.023(\sigma_{0.2}/\sigma_{cr})$	For SHS and RHS the proposed magnitude gave good predictions
Kaitila [31]	Cold-formed steel lipped channels	Numerical	Eigenmodes	0 to h/200 where h is the web height.	No general guidelines emerged from the study.
Dubina and Ungureanu [32]	Cold-formed steel channels and lipped channels	Numerical	Eigenmodes (1st and 5th) and measured imperfections.	[28]	Actual distribution gave the best results when used in numerical modelling. Schafer and Peköz's [28] proposal was found 'helpful'.
Cruise and Gardner [33]	Hot-rolled and cold-formed stainless steel angles and hollow sections	Experimental	Half-sine wave	Specific values of α to be used in [26]	Dawson and Walker's [26] proposal has been calibrated for stainless steel sections considering the effects of manufacturing process.

Table 6: Load-deformation results using imperfection amplitude from Schafer and Peköz's [28] proposed model.

Designation	Imperfection amplitude ω_0 (mm)	Eigenmode 1		Eigenmode 2		Eigenmode 3	
		FE F_u / Test F_u	FE δ_u / Test δ_u	FE F_u / Test F_u	FE δ_u / Test δ_u	FE F_u / Test F_u	FE δ_u / Test δ_u
L 25 × 25 × 3	0.15	0.85	0.68	0.85	0.82	0.90	1.22
L 30 × 30 × 3	0.18	0.88	0.84	0.90	1.03	0.96	1.69
L 40 × 40 × 3	0.24	0.92	0.79	0.93	0.91	0.99	1.29
L 40 × 40 × 3	0.24	0.94	1.01	0.94	0.96	1.00	1.36
L 50 × 50 × 3	0.30	0.96	1.34	1.01	1.68	1.13	2.33
L 60 × 60 × 3	0.36	1.02	1.83	1.10	1.90	1.24	2.38
C 50 × 25 × 3	0.21	0.91	0.98	0.91	0.88	0.92	1.13
C 80 × 40 × 3	0.40	0.90	1.02	0.92	0.89	0.97	1.33
C 100 × 50 × 3	0.53	0.92	1.04	0.94	0.93	1.02	1.64
C 100 × 50 × 3	0.53	0.95	1.09	0.95	0.96	1.00	1.61
C 150 × 50 × 3	0.83	0.88	1.14	0.86	1.07	0.90	0.95
C 50 × 50 × 3	0.30	0.94	1.17	0.97	1.08	1.02	1.36
CL 100 × 50 × 20 × 3	0.53	0.95	1.20	0.90	0.99	0.91	1.15
CL 150 × 50 × 20 × 3	0.83	0.98	1.32	1.04	1.81	0.99	1.42
CL 150 × 65 × 20 × 3	0.83	1.03	1.62	0.99	1.50	1.01	1.66
CL 200 × 75 × 25 × 3	1.13	1.03	1.42	1.07	1.75	1.04	1.68
CL 33 × 17 × 7 × 1	0.17	0.90	0.83	0.93	1.03	0.90	0.92
CL 50 × 17 × 7 × 1	0.28	1.03	1.27	1.08	1.69	1.04	1.25
CL 50 × 22 × 7 × 1	0.28	1.01	1.04	0.98	0.90	0.99	1.12
CL 68 × 25 × 8 × 1	0.38	1.04	1.71	1.01	1.52	1.02	1.71
I 50 × 50 × 3 × 3	0.27	0.79	0.45	0.80	0.61	0.82	0.81
I 50 × 100 × 3 × 3	0.26	0.89	1.06	0.89	1.10	0.91	1.14
I 100 × 50 × 3 × 3	0.57	0.83	0.65	0.83	0.66	0.85	0.76
I 100 × 75 × 3 × 3	0.57	0.86	0.71	0.87	0.76	0.86	0.83
I 100 × 100 × 3 × 3	0.57	0.94	1.44	0.99	1.42	1.01	1.70
I 150 × 100 × 3 × 3	0.87	0.97	1.69	0.98	1.54	1.05	1.54
I 200 × 100 × 3 × 3	1.17	0.94	1.63	0.96	1.56	0.99	1.44
I 200 × 150 × 3 × 3	1.17	1.02	1.58	1.01	1.67	0.99	1.47
I 160 × 80 × 10 × 6	0.83	0.95	0.52	0.96	0.46	0.95	0.48
I 160 × 160 × 10 × 6	0.84	0.99	0.65	0.95	0.48	0.99	0.61
I 320 × 160 × 10 × 6	1.80	0.97	0.85	0.98	0.73	1.00	0.92
I 160 × 160 × 10 × 6	0.84	0.95	0.65	0.93	0.55	0.95	0.66
All Sections	**Average**	**0.94**	**1.10**	**0.95**	**1.12**	**0.98**	**1.30**
	COV	**0.07**	**0.34**	**0.07**	**0.38**	**0.08**	**0.34**

Table 7: Load-deformation results using imperfection amplitude from Gardner and Nethercot's [22] proposed model.

Designation	Imperfection amplitude ω_0 (mm)	Eigenmode 1		Eigenmode 2		Eigenmode 3	
		FE F_u / Test F_u	FE δ_u / Test δ_u	FE F_u / Test F_u	FE δ_u / Test δ_u	FE F_u / Test F_u	FE δ_u / Test δ_u
L 25 × 25 × 3	0.02	0.90	1.00	0.92	1.58	0.96	1.76
L 30 × 30 × 3	0.02	0.97	1.20	0.96	1.51	1.02	2.56
L 40 × 40 × 3	0.04	1.00	1.10	0.99	1.00	1.05	1.82
L 40 × 40 × 3	0.04	1.03	1.29	1.05	1.45	1.13	2.31
L 50 × 50 × 3	0.07	1.03	1.29	1.08	1.61	1.20	2.55
L 60 × 60 × 3	0.10	1.06	1.24	1.16	1.77	1.31	2.30
C 50 × 25 × 3	0.02	0.95	1.29	0.96	1.34	0.95	1.31
C 80 × 40 × 3	0.04	1.01	1.15	0.99	1.18	1.03	1.27
C 100 × 50 × 3	0.07	1.01	0.97	1.01	1.03	1.07	1.23
C 100 × 50 × 3	0.07	1.06	1.00	1.04	1.07	1.10	1.22
C 150 × 50 × 3	0.07	0.99	0.86	0.95	0.86	0.98	0.88
C 50 × 50 × 3	0.07	1.02	1.03	1.02	1.04	1.03	1.06
CL 100 × 50 × 20 × 3	0.02	1.02	1.27	1.00	1.19	1.00	1.23
CL 150 × 50 × 20 × 3	0.06	1.00	0.93	1.06	1.72	0.99	1.18
CL 150 × 65 × 20 × 3	0.06	1.05	1.19	1.02	1.26	1.05	1.58
CL 200 × 75 × 25 × 3	0.11	1.02	1.14	1.08	1.92	1.07	1.73
CL 33 × 17 × 7 × 1	0.01	0.98	0.89	0.99	1.03	0.98	0.96
CL 50 × 17 × 7 × 1	0.02	1.04	1.00	1.07	0.74	1.05	0.98
CL 50 × 22 × 7 × 1	0.02	1.01	1.00	1.01	0.87	1.03	1.14
CL 68 × 25 × 8 × 1	0.04	1.05	1.31	1.02	1.44	1.04	1.70
I 50 × 50 × 3 × 3	0.01	0.89	1.21	0.89	1.18	0.91	1.21
I 50 × 100 × 3 × 3	0.06	0.94	1.12	0.93	1.21	0.95	1.28
I 100 × 50 × 3 × 3	0.03	0.91	1.10	0.91	1.10	0.92	1.27
I 100 × 75 × 3 × 3	0.03	0.96	1.08	0.96	1.07	0.96	1.08
I 100 × 100 × 3 × 3	0.06	1.04	1.45	1.06	1.67	1.09	1.83
I 150 × 100 × 3 × 3	0.06	1.06	1.20	1.13	1.38	1.18	1.55
I 200 × 100 × 3 × 3	0.11	1.02	1.00	1.05	1.09	1.07	1.07
I 200 × 150 × 3 × 3	0.14	1.03	1.12	1.04	1.03	1.08	0.99
I 160 × 80 × 10 × 6	0.03	1.03	0.80	1.02	0.76	1.02	0.75
I 160 × 160 × 10 × 6	0.03	1.05	1.03	1.06	1.03	1.08	1.15
I 320 × 160 × 10 × 6	0.14	1.01	0.81	1.01	0.75	1.02	0.85
I 160 × 160 × 10 × 6	0.05	0.99	1.00	0.99	0.93	0.99	1.02
All Sections	**Average**	**1.00**	**1.10**	**1.01**	**1.21**	**1.04**	**1.40**
	COV	**0.05**	**0.14**	**0.06**	**0.26**	**0.08**	**0.35**

Table 8: Load-deformation results obtained from FE models of I section stub columns with and without residual stresses.

Designation	Test Results		Without Residual Stress		With Residual Stress	
	F_u (kN)	δ_u (mm)	FE F_u / Test F_u	FE δ_u / Test δ_u	FE F_u / Test F_u	FE δ_u / Test δ_u
50 × 50 × 3 × 3	151.8	2.40	0.89	1.21	0.89	1.19
50 × 100 × 3 × 3	190.7	0.73	0.94	1.12	0.94	1.18
100 × 50 × 3 × 3	170.6	1.34	0.91	1.10	0.92	1.22
100 × 75 × 3 × 3	199.2	1.07	0.96	1.08	0.97	1.17
100 × 100 × 3 × 3	201.5	0.49	1.04	1.45	1.05	1.55
150 × 100 × 3 × 3	200.0	0.61	1.12	1.20	1.15	1.38
200 × 100 × 3 × 3	206.8	0.80	1.02	1.00	1.06	1.05
200 × 150 × 3 × 3	230.4	0.89	1.03	1.12	1.05	1.22
All Sections		**Average**	**0.99**	**1.16**	**1.00**	**1.24**
		COV	**0.08**	**0.11**	**0.09**	**0.12**

Table 9: Summary of the predictions for peak loads for all stub columns considered.

Cross-section type	Production process	No. of sources	No. of stub columns	FE F_u / Test F_u	
				Mean	COV
Angle	Press-braking	1	12	1.04	0.06
Channel	Press-braking	1	11	1.03	0.04
Lipped Channel	Press-braking	2	22	1.01	0.05
I section	Welded	2	20	1.04	0.09
SHS	Roll-forming and Press-braking	6	42	1.02	0.11
RHS	Roll forming and Press-braking	4	29	0.97	0.07
All sections	**All possible processes**	**8**	**136**	**1.01**	**0.08**

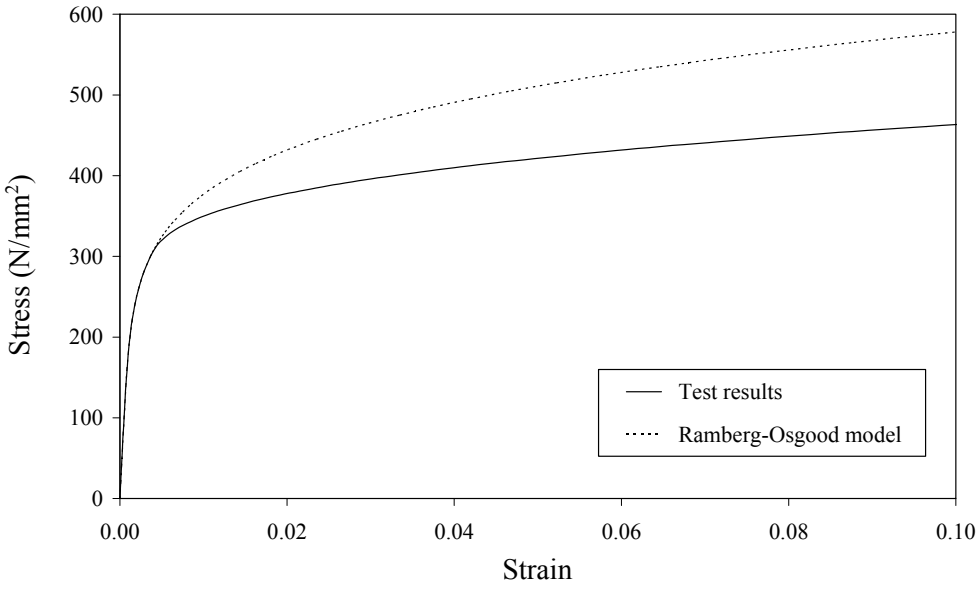

Figure 1: Comparison between the measured stress-strain curve and the Ramberg-Osgood material model for an austenitic Grade 1.4301 tensile coupon with $\sigma_{0.2}$ = 296 N/mm^2 and n = 5.8.

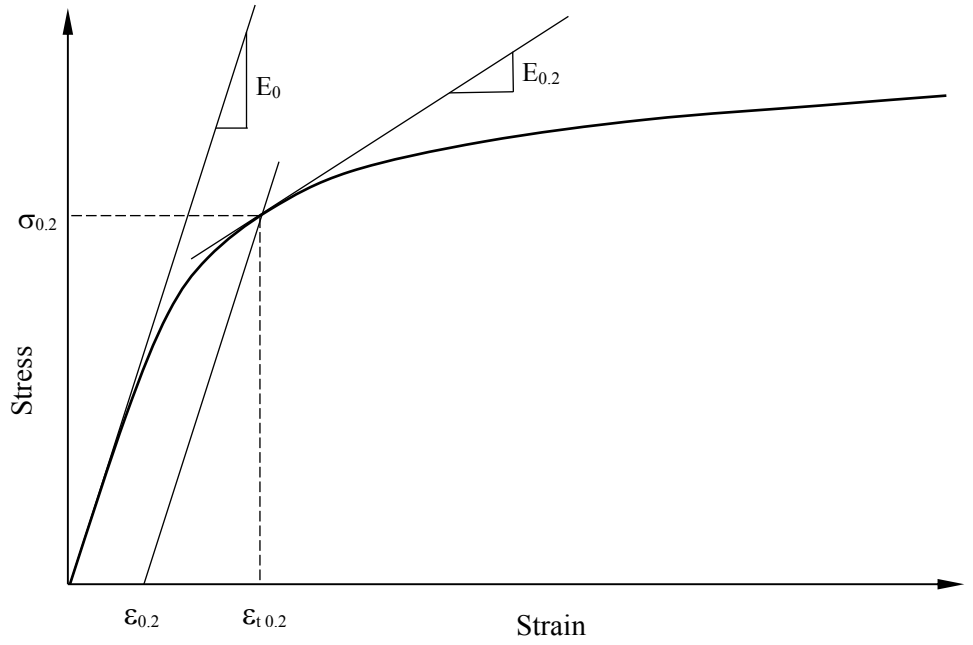

Figure 2: Schematic diagram explaining development of modified Ramberg-Osgood Equation.

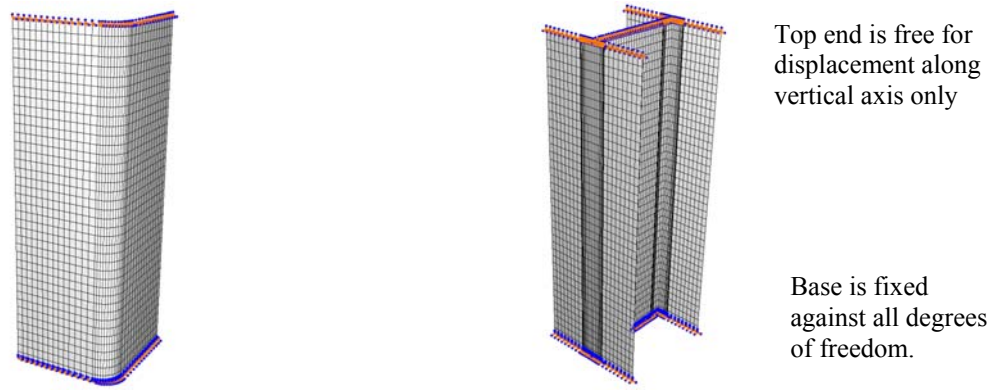

Figure 3: Typical boundary conditions applied to the stub columns.

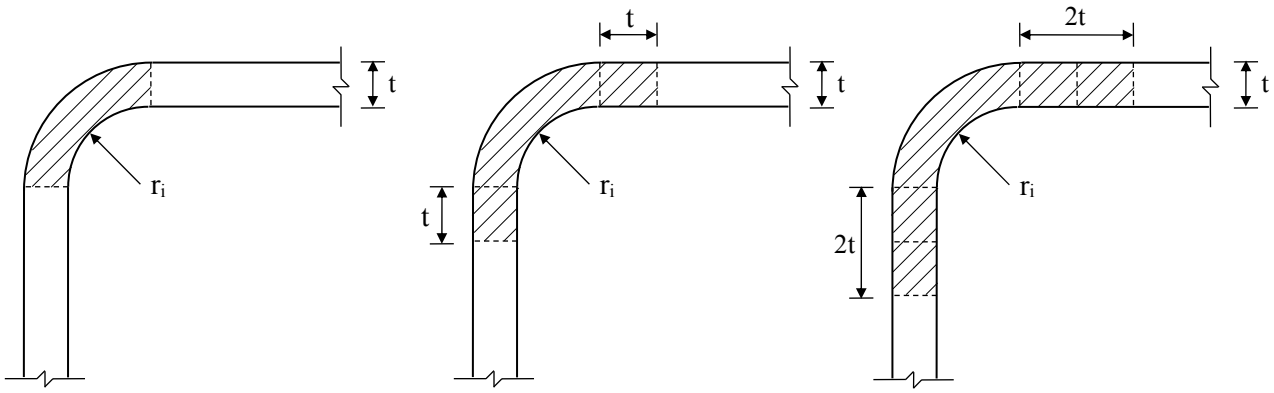

(a) Corner region only (b) Corner region plus t (c) Corner region plus 2t

Figure 4: Different cases considered to study the extent of corner enhancement.

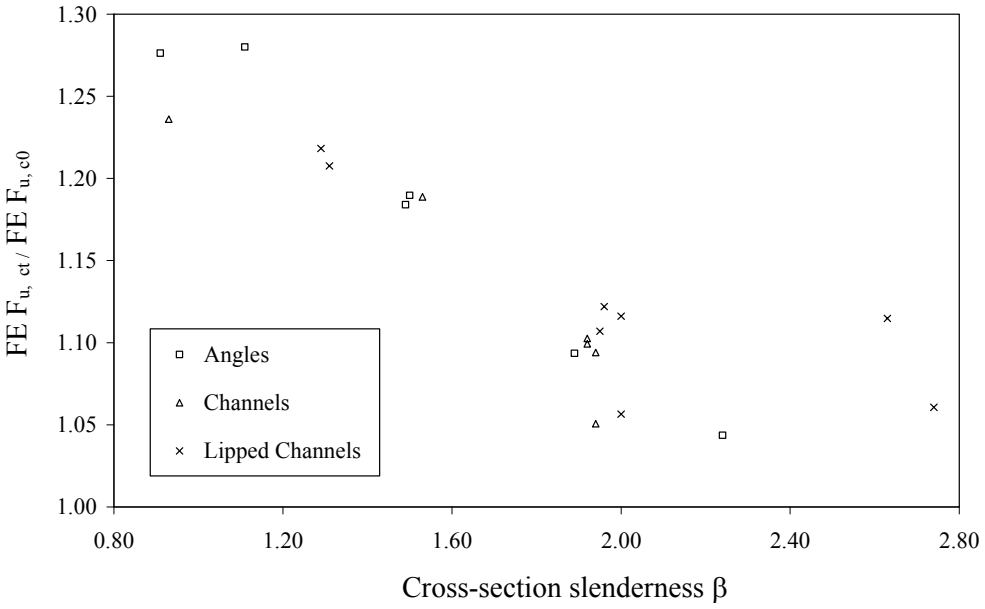

Figure 5: Variation of the effect of corner enhancement with cross-section slenderness β.

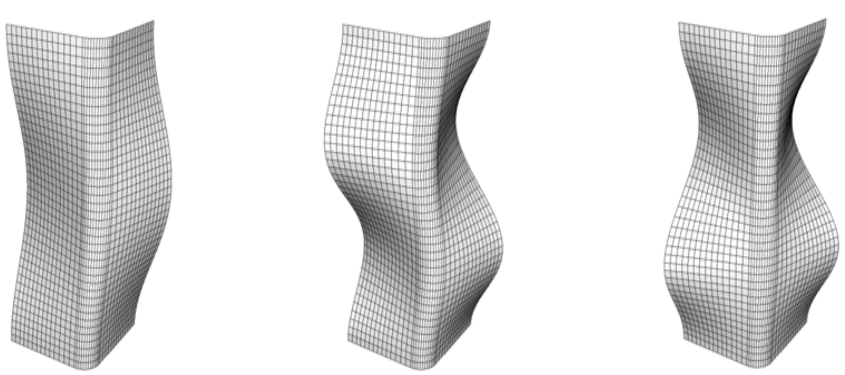

Eigenmodes 1, 2 and 3 for L 25 × 25 × 3

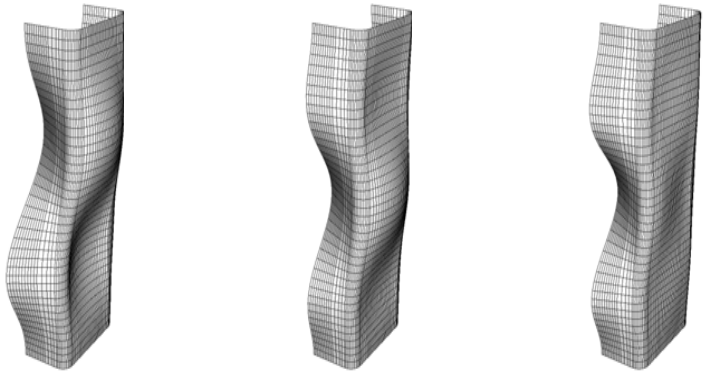

Eigenmodes 1, 2 and 3 for C 50 × 25 × 3

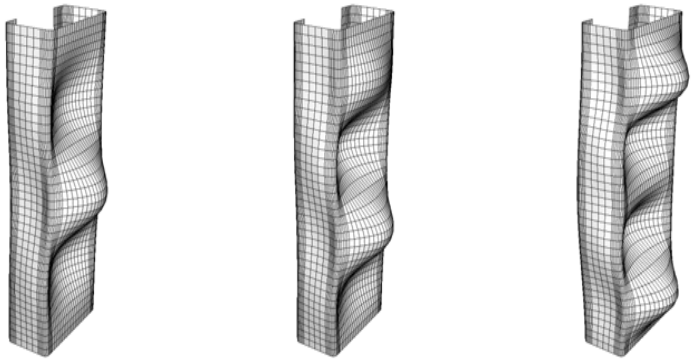

Eigenmodes 1, 2 and 3 for CL 100 × 50 × 20 × 3

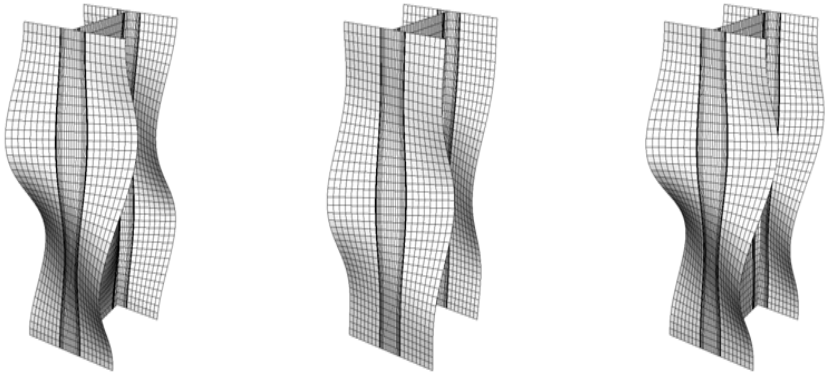

Eigenmodes 1, 2 and 3 for I 50 × 50 × 3 × 3

Figure 6: Typical Eigenmodes obtained by performing elastic analysis for stainless steel open sections.

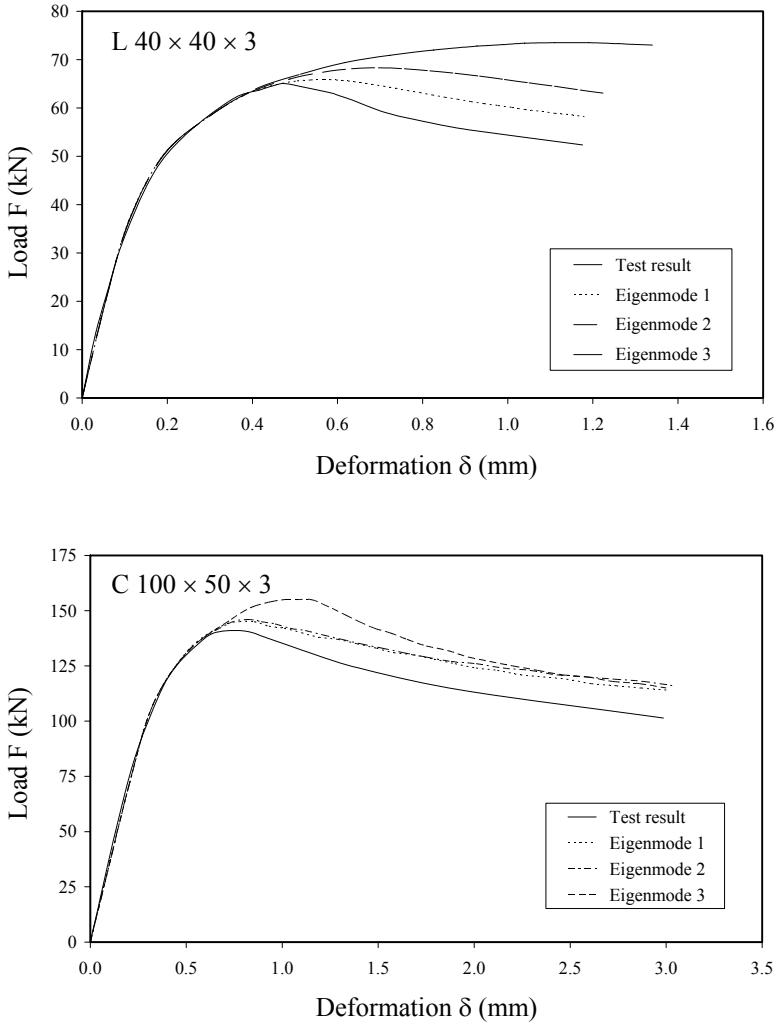

Figure 7: Typical variations in load-deformation behaviour of stub columns as a result of using different imperfection distributions (Eigenmodes).

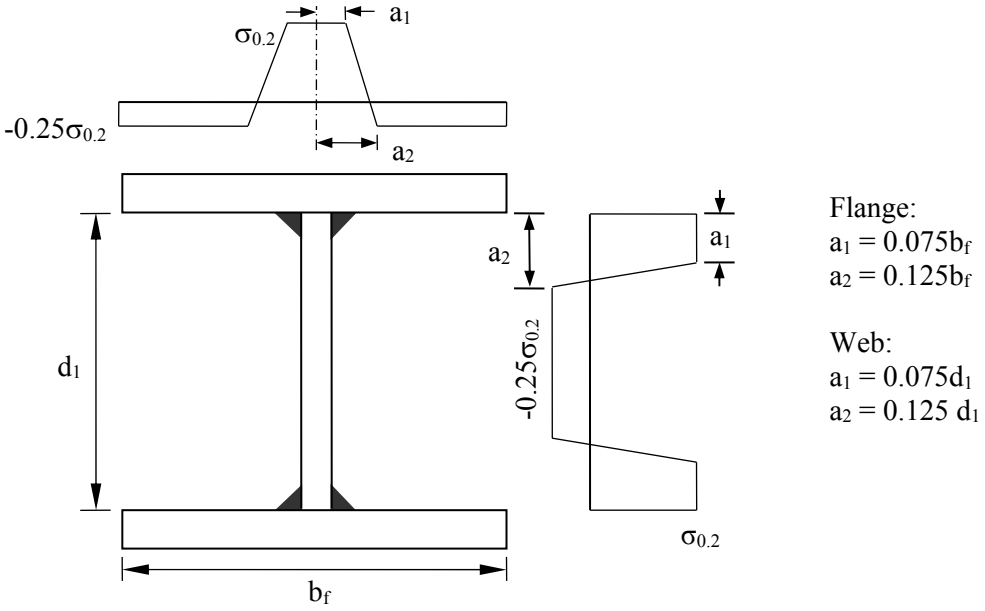

Figure 8: Assumed residual stress distribution for welded I sections.

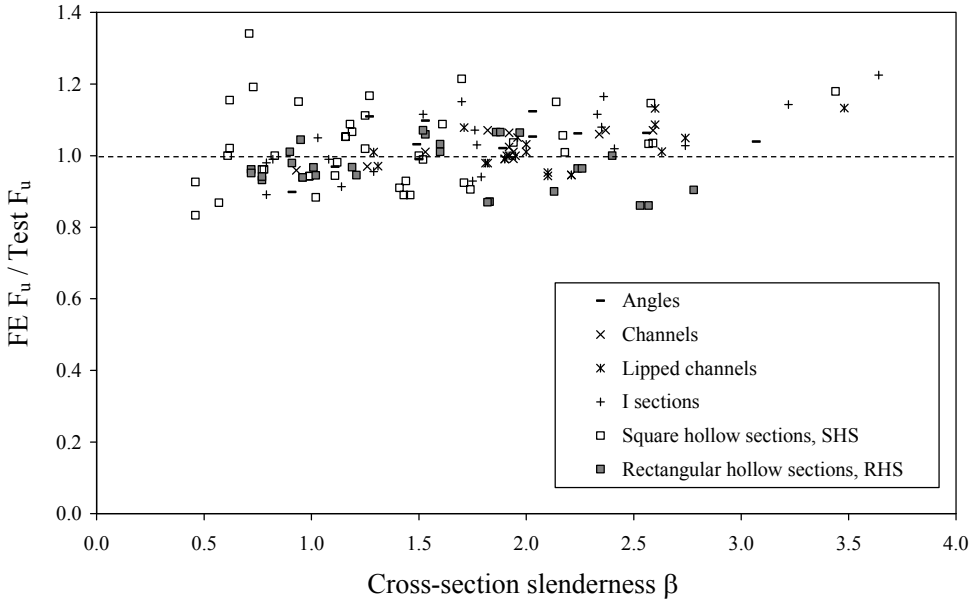

Figure 9: Comparison of the FE predictions for stub column peak load F_u with test results.

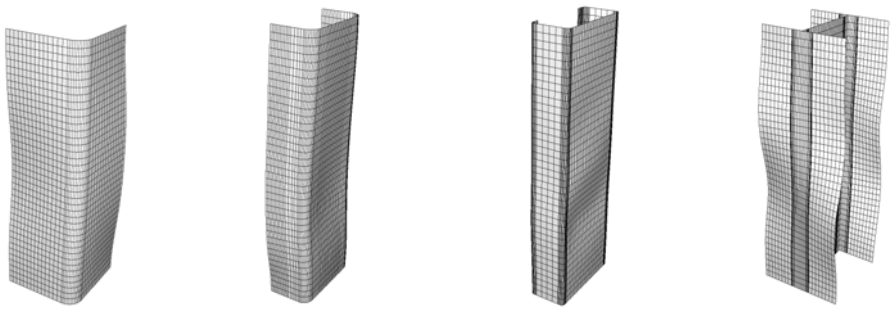

Figure 10: Typical failure modes obtained for different cross-section types.